

Numerical simulation of a 100-ton ANFO detonation

P. W. Weber · K. K. Millage · J. E. Crepeau ·
H. J. Happ · Y. Gitterman · C. E. Needham

Received: 28 October 2013 / Revised: 9 December 2014 / Accepted: 10 December 2014 / Published online: 21 December 2014
© Springer-Verlag Berlin Heidelberg 2014

Abstract This work describes the results from a US government-owned hydrocode (SHAMRC, Second-Order Hydrodynamic Automatic Mesh Refinement Code) that simulated an explosive detonation experiment with 100,000 kg of Ammonium Nitrate–Fuel Oil (ANFO) and 2,080 kg of Composition B (CompB). The explosive surface charge was nearly hemispherical and detonated in desert terrain. Two-dimensional axisymmetric (2D) and three-dimensional (3D) simulations were conducted, with the 3D model providing a more accurate representation of the experimental setup geometry. Both 2D and 3D simulations yielded overpressure and impulse waveforms that agreed qualitatively with experiment, including the capture of the secondary shock observed in the experiment. The 2D simulation predicted the primary shock arrival time correctly but secondary shock arrival time was early. The 2D-predicted impulse waveforms agreed very well with the experiment, especially at later calculation times, and prediction of the early part of the impulse

waveform (associated with the initial peak) was better quantitatively for 2D compared to 3D. The 3D simulation also predicted the primary shock arrival time correctly, and secondary shock arrival times in 3D were closer to the experiment than in the 2D results. The 3D-predicted impulse waveform had better quantitative agreement than 2D for the later part of the impulse waveform. The results of this numerical study show that SHAMRC may be used reliably to predict phenomena associated with the 100-ton detonation. The ultimate fidelity of the simulations was limited by both computer time and memory. The results obtained provide good accuracy and indicate that the code is well suited to predicting the outcomes of explosive detonations.

Keywords SHAMRC · Modeling · High explosive · Detonation · Hydrocode · Secondary shock

1 Introduction

Numerical prediction of the air blast environment due to explosive detonation is an important problem with applications in multiple industries including defense, loss prevention, and impact engineering. Numerical simulations are advantageous in that large-scale explosive experiments carry an inherent degree of risk and also a high monetary cost, and cannot encompass every possible scenario. Additionally, numerical simulations are often the only practical tool available for predicting effects for which experimental data are limited, or not available (or desired) a priori. For example, Luccioni et al. [1] used the code AUTODYN-2-D to analyze the blast effects and resultant damage to buildings for a terrorist attack, comparing code results to a real damage scenario, which allows for use of the code to predict the results of theoretical attacks. Pierazzo and Melosh [2] used the hydrocode

Communicated by F. Zhang and H. Kleine.

P. W. Weber · K. K. Millage
Applied Research Associates, Inc., 801 N. Quincy St.,
Ste. 700, Arlington, VA 22203-1730, USA

J. E. Crepeau · H. J. Happ · C. E. Needham
Applied Research Associates, Inc., 4300 San Mateo Blvd.,
Ste. A220, Albuquerque, NM 87110-1229, USA

Y. Gitterman
Geophysical Institute of Israel, P.O.B. 182, Lod 71100, Israel

Present address:
P. W. Weber (✉)
Institute for Defense Analyses, 4850 Mark Center Dr., Alexandria,
VA 22311-1882, USA
e-mail: pweber@ida.org

CTH to analyze the results of the Chicxulub asteroid event, and were able to use the tool to predict the effect of impact angle.

For numerical simulations to be of value, codes used for prediction of air blast phenomena must be compared and validated against experimental data. Once a code is shown to adequately characterize the explosive detonation environment, useful follow-on studies may be conducted. For example, if a code predicts air blast transport well compared to experimental data, it may be used to postulate the air blast behavior inside complex structures such as tunnels [3], and numerical flow visualization may be used to explore phenomena that are difficult to observe experimentally. Once a high degree of confidence is obtained, code results may also be used in applications such as analyzing effects of protective barriers [4] and analyzing building collapse under blast loads [5].

The US government-owned hydrocode SHAMRC (Second-order Hydrodynamic Automatic Mesh Refinement Code [6]) is used to model the air blast effects of explosives (among other applications). SHAMRC has been extensively used and validated against a wide array of experimental data, having been used for predictions in a large variety of high explosive experiments [7]. The term “hydrocode” is often used to characterize codes like SHAMRC, as a hydrocode refers to a computer program used to study the dynamic response of materials and structures to impulse (blast) and impact [8]. SHAMRC solves the Euler equations on a structured mesh using second-order differencing in both space and time, and is fully conservative of mass, momentum, and energy. Explosive burn models in SHAMRC allow for the simulation of both early and late stages of explosive detonations, and multiple explosive materials are available.

A unique characteristic of certain (geometry-dependent) conventional solid explosions is the formation of a secondary shock [9]. In conventional explosions, after the primary shock has formed, the high momentum density of the expanding detonation products causes an overexpansion of the interior, which results in the formation of a backward-facing shock. This backward-facing shock converges on the detonation point and reflects from the center. The secondary shock is observed experimentally at overpressure stations as a secondary rise in pressure after the primary shock has passed. The secondary shock pressure rise is significantly smaller in magnitude than the primary shock pressure rise, but is sufficiently well defined to be observable.

Empirical formulas for relating air blast parameters to charge size and type exist, such as the US Army Technical Manual (TM) 5-855-1 [10] and other formulas that fit curves to air blast parameters such as those described in Needham [9] and Sochet et al. [11]. These empirical formulas have the advantage of allowing for rapid calculations of global parameters of interest using limited input information. However, there are numerous disadvantages to using simple empirical

formulas. They cannot provide information such as detailed waveform shape, or account in detail for the effect of unique charge geometries and/or complex obstacles on the air blast wave. Empirical formulas also cannot provide the detailed flow visualization that is allowed by numerical simulation.

1.1 Brief experiment overview

The explosion experiment that is to be modeled for this report was conducted at the Sayarim Military Range in Israel in January 2011 [12]. The purpose of the detonation was the calibration of International Monitoring System infrasound stations. The charge was a surface detonation of 102,080 kg nominal weight on dry alluvial sediments. Extensive experimental data were collected, including output from pressure gauges, accelerometers, seismometers, regular and high-speed video cameras. Since only one detonation was conducted, statements pertaining to test repeatability could not be made.

Figure 1 shows a photograph of the final completed charge prior to detonation, and Fig. 2 shows the design scheme for the charge. The charge was composed of 115 “big bags” of ANFO and 208 M-15 mines. Each “big bag” of Ammonium Nitrate–Fuel Oil (ANFO) consisted of 870 kg of pre-mixed 94 % Ammonium Nitrate and 6 % Fuel Oil (Detonation Velocity: 2,400 m/s, density: 0.80–0.81 g/cc). Each M-15 mine contained 10 kg of explosive Composition B, and the mines were used as boosters (i.e., to add energy to aid in the propagation of the detonation wave).

The design scheme for the charge was intended to satisfy multiple criteria. First, the charge was intended to be approximately hemispherical in shape, with sharp corners avoided. Second, the detonation direction was intended to be upward.



Fig. 1 Experimental charge geometry. Charge consists of four layers of ANFO bags bounded with a steel band for charge compactness and stability. This photograph is reprinted from Fig. 1 of [12] with permission from Springer

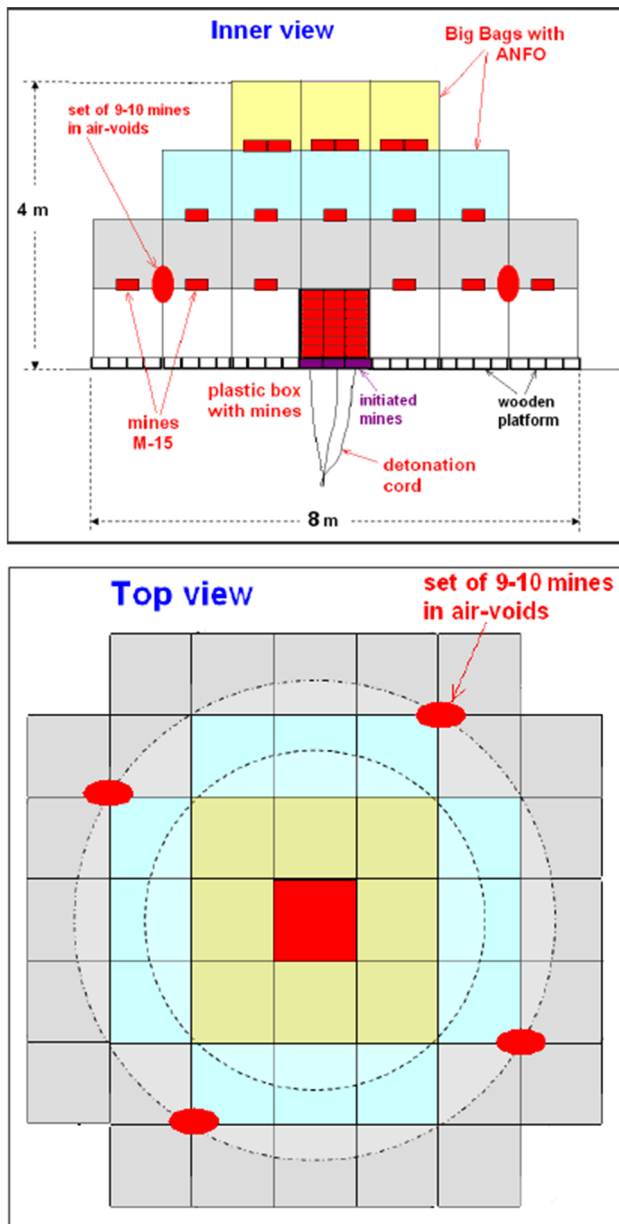


Fig. 2 Design scheme for the experimental charge. This diagram is reprinted from Fig. 1 of [12] with permission from Springer

This upward detonation was achieved by placing most of the M-15 mines in several dense layers in a plastic box at the center of the charge at ground level (the main booster), with detonation cord and inserted detonators attached to several mines in the lowest layer (the initiation points). Third, air voids between the charge layers were minimized. Finally, the detonation wave front propagating upward was reinforced by placing single M-15 mines beneath each bag (except for the upper layer where two M-15 mines were placed beneath each bag) and placing additional mines in air voids in four corners of the first layer (see Fig. 2). The upward propagation of the detonation wave front is important to ensure less explosive

energy coupled to the ground and more energy radiated to the atmosphere and thus observation of infrasound signals at larger distances.

The charge was detonated on January 26, 2011, air temperature 13 °C, with a local altitude of 558 m. No significant surface wind was recorded at the time of the experiment. Although there were numerous experimental data collection devices present during the experiment, the devices of interest to this report were overpressure gauges at 103, 203, 303, 405, 513, and 580 m from ground zero. The gauges with disc type baffles were mounted on steel rods ~ 1.5 m above the surface providing side-on free-field over-pressure measurements with sampling rate of 2 MHz. These overpressure gauges were arranged in a line which was directed roughly southeast from ground zero.

Further details concerning the experiment for the interested reader, including a detailed description of the experimental setup and a discussion of the experimental results, may be found in [12].

2 Methods

2.1 Simulation setup: two-dimensional axisymmetric (2D)

As an initial study, a 2D axisymmetric idealized simulation of the Sayarim 100-ton ANFO detonation was run. Figure 3 shows the initial 2D setup in SHAMRC. The 2D calculation utilized a SHAMRC-defined cylindrical calculation domain, which means that the *x*-axis shown in Fig. 3 represents radial distance from the center of the detonation, and the *y*-axis represents height (i.e., the simulation is axisymmetric, not planar). Gravity is accounted for in the calculation, which is critical as the radius of the shock front becomes large. SHAMRC uses the 1962 standard atmosphere [13]. For the simulation, the temperate atmosphere was used, and the local altitude of 558 m was accounted for. The Landau–Stanyukovich–Zeldovich and Kompaneets (LSZK) form of the equation of state was used in SHAMRC for the detonation products [9]. The bottom boundary condition was a solid surface (reflective boundary condition), and the left boundary condition was reflective (symmetry boundary condition). The top and right boundary conditions were rezone boundary conditions (to be discussed later).

An immediate observation from Fig. 3 is that a deviation from the true three-dimensional (3D) geometry is apparent. For the 2D simulation, the total mass of CompB (from the landmines) was assumed to be hemispherical and centered at the origin. The total mass of the ANFO was also assumed to be hemispherical, and surrounded the CompB. The explosive burn was initiated at the origin, which means that the CompB burnt first and initiated the ANFO. The total explosive mass was the same between the experiment and simulation.

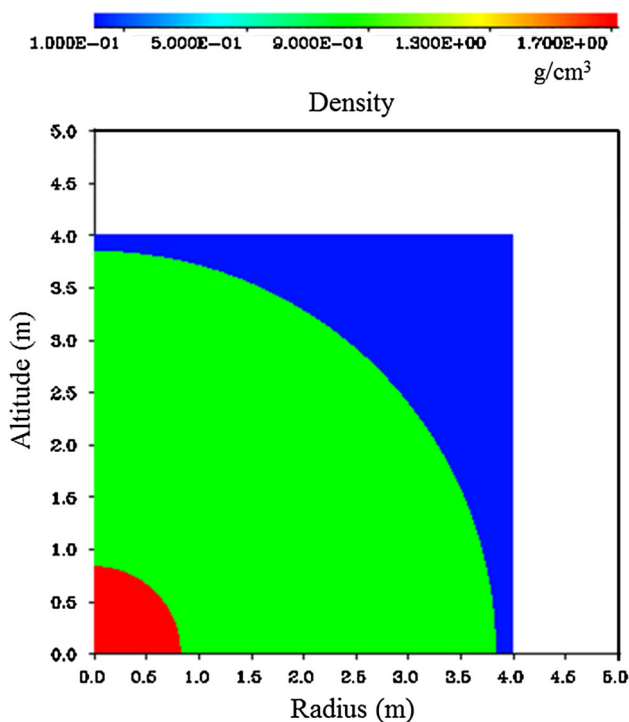


Fig. 3 2D cylindrical simulation setup in SHAMRC, as visualized by the code. The *red* represents CompB, the *green* represents ANFO

Despite the assumptions made for the 2D geometry, this simulation was expected to capture the major experimental phenomena observed. Variations are expected to occur, but the gross features should be apparent and the results are expected to yield insights.

The 2D simulation exploited SHAMRC's standard shock rezone feature. The standard shock rezone in SHAMRC determines when the shock wave is near a boundary, then increases the total domain size while retaining the total number of zones, which means that the zone size gradually increases as the calculation proceeds. The zone size increase at each rezone is 5%. The original mesh information is remapped to the larger mesh. The calculation proceeds until the shock reaches the new boundary, another remap occurs, until the simulation stop time is reached. The result of this algorithm is that the initial zone size is very small, which allows for capture of critical features such as the explosive burn, since all zones are contained in a small initial domain. For example, as shown in Fig. 3, the initial domain size was 4 m², with all zones in the mesh contained in this domain. When the calculation terminated at 3 s physical time, the domain size was approximately 800 m², but contained the same number of zones.

Two different mesh sizes were run in 2D: a coarse mesh and a fine mesh. As mentioned before, the coarsely zoned calculation was run to identify any potential simulation issues. All calculations were run in parallel on DoD high-

performance computing (HPC) platforms, where many users contend for HPC resources. Smaller calculations require a smaller number of processors, and turnaround is generally quicker. The coarse mesh contained 4,000 zones in each direction, or 16 million total zones. The fine mesh contained 15,000 zones in each direction, or 225 million total zones. SHAMRC guidance regarding the zone size for high explosive simulations is [6]:

$$\text{Zone size in cm} = (40 \text{ cm}) (KT)^{1/3}$$

In the equation above, KT is the yield of the detonation in kilotons of TNT. This SHAMRC guidance is based upon user feedback and analysis over decades of use of the code. Using the above equation, for the 102-ton ANFO detonation, the SHAMRC-recommended zone size is 19 cm.

The 2D simulations also contained tracer particles, which move with the flow, but do not interact with it, and are a helpful visualization tool. For this particular calculation, tracer particles were placed at the CompB/ANFO interface and at the ANFO/Air interface at the beginning of the calculation. As the calculation evolves, the user may visualize the paths that these particles take in the flow field.

2.2 Simulation setup: 3D

A 3D simulation was run of the Sayarim 100-ton ANFO detonation. The 3D simulation captured the major geometrical features of the experimental geometry. Figure 4 shows the 3D simulation setup in SHAMRC. This calculation used same atmosphere, ground altitude, and equation of state as the 2D calculation. It is evident from Fig. 4 that some assumptions in terms of geometry still had to be made to make the calculation feasible. The geometry was quarter-symmetric; (symmetry) boundary conditions were used across the planes defined by the intersection of the x - z and y - z axes. The bottom boundary condition for the z -plane (plane defined by the intersection of the x - y -axes) was a solid surface (reflective boundary condition). All other boundary conditions were termination boundary conditions (to use a manual rezone, to be discussed later). The consequence of the quarter-symmetry assumption is that the total mesh size was reduced by a factor of four. The true experimental geometry was not quarter-symmetric, since symmetry was destroyed by the placement of differing numbers of landmines in the air voids at slightly off-symmetric locations (see Fig. 2, which states that a "set of 9–10 mines in air-voids" was placed in the charge; the simulation assumed the overall average of 9.5 mines in the air void). However, the bulk of the experimental geometry demonstrated symmetry, and the explosive mass that violated the quarter-symmetry assumption was small compared to the total explosive mass, so the quarter-symmetric assumption of the simulation geometry is reasonable. As with the 2D simulation, the masses of

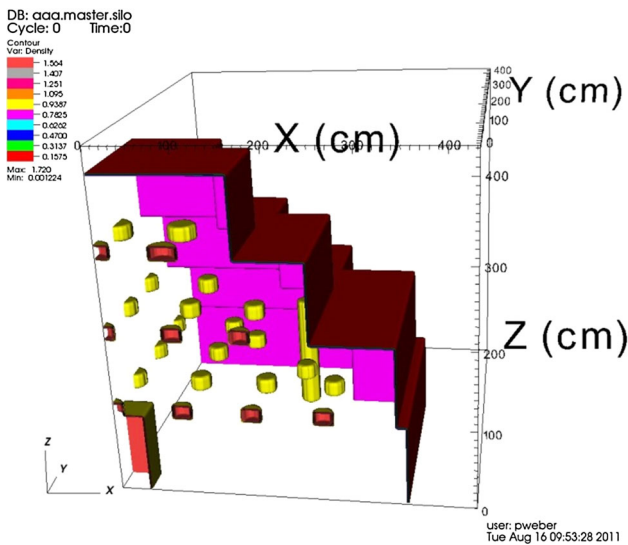


Fig. 4 3D simulation setup in SHAMRC, as visualized by the code

the CompB and the ANFO were the same between the experiment and the 3D simulation.

At the current time, SHAMRC does not have a 3D analog to the 2D standard (automatic) shock rezone. Therefore, the calculation was manually rezoned in stages. Zone size issues necessitate the use of a manual rezone in 3D. To elaborate, the final domain size at the point where the experimental data terminates (approximately 3 s physical time) is approximately 800 m based on experimental data (the furthest sensor was at 580 m, but the domain must extend beyond this value to capture the entire overpressure wave). If a 3D simulation with 800 zones in each direction (which was the case, to be discussed) is run and no rezone is used, the zone size would be 800 m/800 zones = 1 m/zone, which is unacceptably large for earlier times since only 4 zones would span the initial 4-m charge radius in each direction. Therefore, the initial domain size was small (6 m in all directions, slightly larger than the charge), with all zones contained in this 6-m domain, making the initial zone size much smaller and therefore able to more accurately capture flow features. SHAMRC can stop the calculation when any signal nears a boundary. A new calculation with a domain size twice that of the previous calculation can then be constructed, with results from the previous calculation imported into the new calculation. The zone size increased by a factor of 2 between each stage (except for the transfer from the initial burn stage to the first stage). This process continued until the final domain size was approximately 800 m, for 8 total stages, in addition to an initial burn stage that captured the explosive burn at the beginning of the calculation.

As with the 2D calculation, two different mesh sizes were run for the 3D simulation: a coarse mesh and a fine mesh. The coarse mesh 3D calculation had 800 zones in the *x*-, *y*-,

Table 1 Summary of mesh statistics for 2D and 3D simulations

Calculation	Total number of zones (millions)	Initial zone size (cm)	Final zone size (cm)
2D coarse	16	0.1	20
2D fine	225	0.027	5.3
3D coarse	512	0.75	96
3D fine	1,728	0.5	64

and *z*-directions, for a total mesh size of 512 million zones. The fine mesh calculation had 1,200 zones in the *x*-, *y*-, and *z*-directions, for a total mesh size of 1.728 billion zones. A summary of the mesh statistics for both the 2D and 3D simulations is in Table 1. All initial zone sizes were smaller than the SHAMRC (high explosive) recommended zone size of 19 cm by an order of magnitude for both the 2D and 3D simulations. The final 2D zone size met the recommendation as well. The final 3D zone size fell outside the recommendation, but given the overall size of the mesh used (1.728 billion zones), increasing the mesh size to meet the 19 cm final zone size guideline would require a mesh on the order of 10 billion zones, which exceeded the computational resources available.

3 Results and discussion

3.1 Simulation results: overpressure

Stations (computational overpressure sensors) were placed in the calculations at distances of 103, 203, 303, 405, 513, and 580 m from ground zero, corresponding to the experimental overpressure gauges. The SHAMRC predicted overpressures for both the 2D and 3D simulations are compared to the experimental data in Figs. 5 and 6. Numerical comparisons of selected parameters between experiment and simulation for the 2D simulation only are in Table 2, and numerical comparisons of selected parameters between simulation and experiment for the 3D simulation only are in Table 3. The results in Figs. 5 and 6 and Tables 2 and 3 consider fine mesh calculations only; fine mesh calculations both show greater detail in the overpressure waveforms and follow SHAMRC guidance for sufficient calculation zone size. Further details concerning the use of fine mesh calculations over the coarse mesh calculations appear later in this section.

The first and most prevalent observation from the 2D results is that qualitatively, the results are quite good despite the assumptions made to obtain the 2D geometry. The overpressure waveforms are qualitatively correct, with a sharp rise to peak overpressure corresponding to the arrival of the primary shock, followed by a decay and then, very importantly, a prediction of the secondary shock that was seen

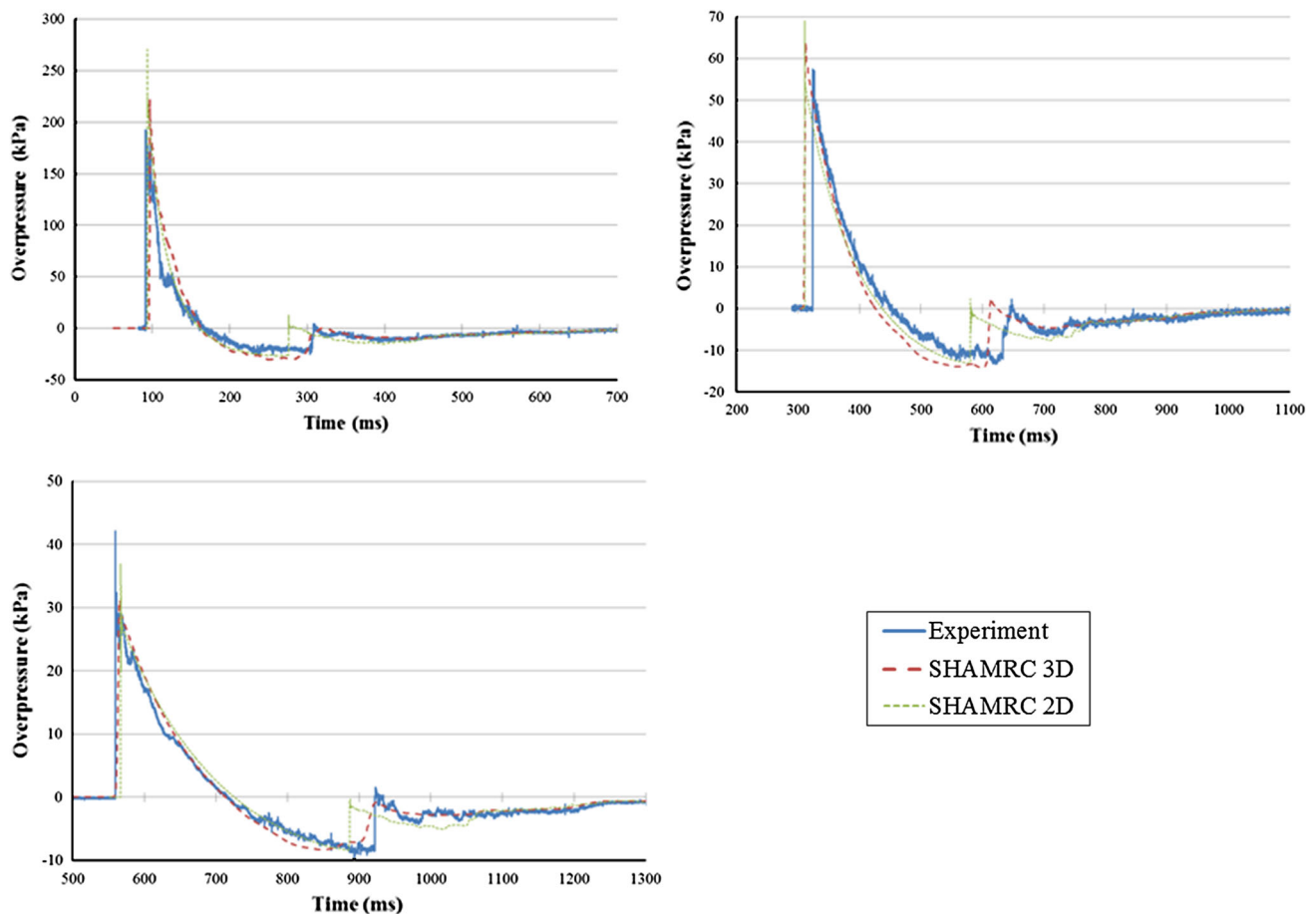


Fig. 5 Overpressure vs. time at sensor 103 m from ground zero (*upper left*), 203 m from ground zero (*upper right*; local terrain variations that were not accounted for in the simulation could account for the early

predicted arrival time of the primary shock), and 303 m from ground zero (*bottom*), 2D and 3D fine mesh simulations

to occur experimentally. The 2D simulation tends to over-predict the magnitude of the peak overpressure, and tends to predict an arrival time of the secondary shock that is earlier than observed experimentally.

The secondary shock arrival time is predicted early in the 2D simulation due to the total mass of the CompB being contained in a hemisphere about the origin (Fig. 3). In the experiment, there was a mass of CompB centered in a column at the origin, but there were also landmines interspersed in the ANFO (Fig. 2). The effect of lumping all of the CompB at the origin for the 2D simulation is that the timing of the energy release into the mesh is altered (although, as mentioned before, since the total mass is the same as experiment, the same total energy is released into the mesh). The timing of the energy release is important because CompB has a higher energy density than ANFO. Therefore, in the 2D simulation, all of the high-energy explosives were burnt first, which altered the formation time of the secondary shock, as interactions of the burnt explosive products with the environment are an integral component of secondary shock formation.

Figure 5, upper right, and Fig. 6, upper right, show primary shock arrival times that are noticeably different from the experimental results. Figure 5, upper right, which is the sensor 203 m from ground zero, shows that SHAMRC predicts an earlier arrival time of the primary shock compared to experiment. Figure 6, upper right, which is the sensor 513 m from ground zero, shows that SHAMRC predicts a later arrival time of the primary shock compared to experiment.

Agreement in primary shock arrival time between simulation and experiment was very close for all other stations. The likely reasons that these two predictions are inconsistent with experiment are (a) the simulations did not account for terrain, and (b) station placement error. In general, the Sayarim Military Range consists of flat desert terrain, although the experimenters did note that there was slight rolling terrain in places. If a sensor is placed on an upward or downward slope, the travel distance of the shock is slightly altered, which affects the arrival time. Even though the shock travels at speeds on the order of sonic velocity, a slight variation in travel distance can result in arrival times altered by a few milliseconds,

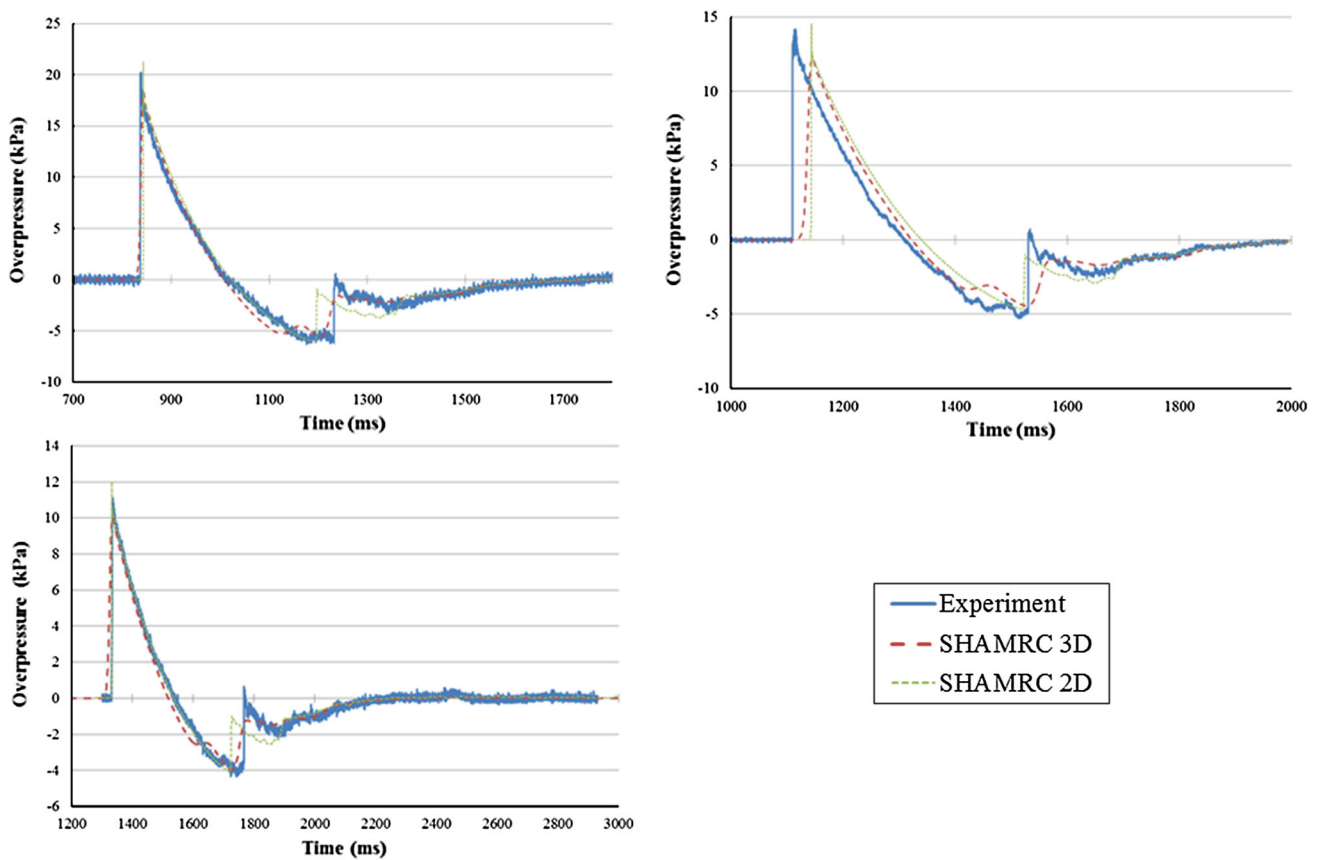


Fig. 6 Overpressure vs. time at sensor 405 m from ground zero (*upper left*), 513 m from ground zero (*upper right*; local terrain variations that were not accounted for in the simulation could account for the late pre-

dicted arrival time of the primary shock) and 580 m from ground zero (*bottom*), 2D and 3D fine mesh simulations

Table 2 Numerical comparison of select parameters between experiment and simulation, 2D

Sensor (m)	Experimental OP_{max} (kPa)	Simulation OP_{max} (kPa)	Percent difference in OP_{max} (%)	Experimental OP_{min} (kPa)	Simulation OP_{min} (kPa)	Percent difference in OP_{min} (%)
103	192.4	270.3	40.5	-26.6	-26.6	0.0
203	57.5	68.9	19.8	-13.4	-13.1	2.2
303	42.1 ^a	36.9	-12.4	-9.7	-8.4	13.4
405	20.2	21.2	5.0	-6.3	-6.1	3.2
513	14.2	14.5	2.1	-5.3	-4.7	11.3
580	11.1	12.0	8.1	-4.3	-4.1	4.7

Only fine mesh simulation results are considered

^aThe raw experimental overpressure data read an OP_{max} of 6.11 psi (42.1 kPa) for this 303-m sensor. However, Table 5 of [12] reports the peak overpressure at this 303-m sensor of 30.16 kPa. If the Table 5 of [12] data is taken as the true peak overpressure, percent difference in OP_{max} is 22.3 % as opposed to -12.4 %

which was seen. Slight experimental measurement error in the actual placement distance of the stations from ground zero can result in deviations of arrival time between experiment and prediction. A curious result from the SHAMRC predictions is that only two of the six stations exhibited arrival times differing from experiment, and the deviations were not systematic. If the arrival time was early for the 203-m sensor, one would expect that it would be early for all following sen-

sors, which was not the case. Instead, the prediction was on time for the 303- and 405-m sensors after being early for the 203-m sensor, then was late for the 513-m sensor, then was on time again for the 580-m sensor. We have no explanation for this.

One final observation from the 2D simulation results is that although the fine mesh calculation took approximately 90 times longer to run in CPU hours compared to the coarse

Table 3 Numerical comparison of select parameters between experiment and simulation, 3D

Sensor (m)	Experimental OP _{max} (kPa)	Simulation OP _{max} (kPa)	Percent difference in OP _{max} (%)	Experimental OP _{min} (kPa)	Simulation OP _{min} (kPa)	Percent difference in OP _{min} (%)
103	192.4	221.3	15.0	−26.6	−30.3	−13.9
203	57.5	63.9	11.1	−13.4	−14.2	−6.0
303	42.1 ^a	31.2	−25.9	−9.7	−8.3	14.4
405	20.2	18.3	−9.4	−6.3	−5.6	11.1
513	14.2	12.3	−13.4	−5.3	−4.5	15.1
580	11.1	10.1	−9.0	−4.3	−4.0	7.0

Only fine mesh simulation results are considered

^aThe raw experimental overpressure data read an OP_{max} of 6.11 psi (42.1 kPa) for this 303-m sensor. However, Table 5 of [12] reports the peak overpressure at this 303-m sensor of 30.16 kPa. If the Table 5 of [12] data is taken as the true peak overpressure, percent difference in OP_{max} is 3.4 % as opposed to −25.9 %

mesh calculation, the results are roughly similar. The only deviation is that a sharp downward spike in the overpressure was seen at 130 ms at the 103-m sensor for the coarse calculation that was not present for the fine calculation. The fine calculation shows greater detail in the overpressure waveform, but as a whole, the fine mesh calculation results essentially fall on top of the coarse mesh calculation results on the overpressure plots. This indicates that the zone resolution for the fine mesh is sufficient—there should be no significant change in results using an even finer mesh.

As with the 2D calculation, the results for the 3D simulation compare well with experimental data. The prediction of the overpressure waveforms is qualitatively correct. The 3D simulation results display generally better quantitative agreement in overpressure compared to experiment than the 2D simulation results. The magnitude of the peak overpressure for the 3D simulation is closer to experiment in most (but not all) cases, and the arrival time of the secondary shock is in line with experimental observations (Figs. 5, 6).

Note that the experimental data at the 103-m range (Fig. 5, upper left) contain a number of oscillations in the decay phase of the initial shock. Such oscillations are not observed on the other waveforms. The probable cause of these oscillations is the impingement of detonation products caused by Rayleigh–Taylor instabilities at this distance. Since they are randomly generated and affect the overpressure, this could be the cause of the observed difference in overpressure for this range. As with the 2D simulation, there were some inconsistencies with the arrival time of the primary shock for the 3D simulation. However, no real trends were observed (as with the 2D simulations), and the differences could easily be due to terrain issues and precision of sensor placement. The overall agreement is excellent.

Some issues related to zone size were observed with the 3D simulations. Even though the 3D simulations contained large numbers of total zones (512 million and 1.728 billion), the fact that these zones had to be divided among three dimen-

sions instead of two meant that the average zone size for the 3D simulations was significantly larger than for the 2D simulations. For example, for the fine mesh calculation initial burn stage, the initial zone size in 3D was 0.5 cm, whereas it was 0.1 cm (coarse) and 0.027 cm (fine) in 2D. The effect of larger zone sizes is seen in the shock resolution. In the 2D simulations, the primary and secondary shocks were fairly well defined, with short rise times (steep slope). However, in 3D, the shock rise times for the primary shock at later times and secondary shock for most times are seen to be longer than experiment (i.e., a more gradual rise to peak overpressure). The reason for this more gradual rise time in 3D is that the numerical shock resolution algorithm in SHAMRC requires a shock to be calculated (“spread out”) over multiple zones—at least three, sometimes more. When these zones are large, as they were in 3D (or with a coarse mesh calculation), the shock is spread out over a larger distance and therefore the rise time is more gradual. This effect is especially prevalent at later times, where the zone sizes in 3D become large.

A significant observation from the 3D simulation results is that although the fine mesh calculation took over 5 times longer to run in CPU hours compared to the coarse mesh calculation, the results are similar. The fine calculation does show slight differences in the trace of the overpressure waveform, but as a whole, the fine mesh calculation results essentially overlay the coarse mesh calculation results on the overpressure plots. As with 2D, this indicates that making the mesh even finer will not change the results significantly.

A major benefit of modeling is the ability to present the numerical data in a form equivalent to flow visualization. Figure 7 shows the result of one such flow visualization for the 3D simulation. In this figure, the shape of the pressure contour for the blast wave is visualized. A major observation is that the interspersed landmines (CompB) in the ANFO significantly affect the shape of the pressure contour at earlier times (when the blast wave front is close to ground zero). For contours a–g in Fig. 7, noticeable non-uniformity in the blast

wave contour exists. Of note, the protrusions (“bumps”) in the contours correspond to the locations of the interspersed landmines in the ANFO. When the CompB detonates, it releases more energy than the ANFO surrounding it, since CompB has a higher energy density than ANFO. This leads to protrusions in the pressure contour. However, at later times (contours h and i in Fig. 7), the protrusions in the blast wave contour gradually smooth out (gradients are relaxed) and the blast wave eventually exhibits a classical hemispherical shape.

Flow visualization techniques may also be used to visualize density contours of the detonation products, which are shown in Fig. 8. In this figure, the 3D simulation results were used to generate a 2D slice through the center of detonation. Rayleigh–Taylor instabilities that have formed result in non-uniform variations at the surface of the detonation product–air interface.

3.2 Simulation results: overpressure impulse

The overpressure impulse, also known as the integrated pressure, is a useful metric for yield determination. The final yield estimations for Sayarim calibration explosions (including the one presented here) were based on measured maximal (positive phase) impulse values [12]. The overpressure impulse is defined as the total area under the curve for the variation of overpressure with time [14]. The overpressure impulse calculation starts at the initial shot time and continues until the overpressure returns permanently to zero, thus including both the positive and negative phases. The peak overpressure impulse corresponds to the end of the positive phase. SHAMRC calculates overpressure impulse directly. The predicted variation of overpressure impulse with time for both the fine mesh 2D and fine mesh 3D simulations is plotted against experimental results for select sensors in Fig. 9, and numerical comparisons of select parameters between simulation and experiment are in Table 4. Additionally, Fig. 10 shows a comparison between experiment and simulation for both the overpressure and overpressure impulse as a function of distance from ground zero.

As with the overpressure, the overpressure impulse results in Fig. 9 are seen qualitatively to agree well with experiment for both the 2D and 3D simulations, and the quantitative agreement shown in Table 4 is also good for later times. The shapes of the overpressure impulse curves are correct, and the predicted times for peak overpressure impulse are predicted well. For the 3D simulation, the local variations in the overpressure impulse due to the secondary shock are also predicted well; they are early for the 2D simulations as the secondary shock was predicted early. Figure 10 shows that at further distances from ground zero, quantitative agreement for both 2D and 3D simulations is good.

The most striking difference between simulation and experiment is the predicted peak value of overpressure

impulse for earlier times (closer distances), which is seen to be larger than experiment (Fig. 9), and better predicted by the 2D simulation (Fig. 10). The reason for this difference may be ascertained by observing the overpressure vs. time curves in Fig. 5. In this figure, it is seen that in general, the predicted drop in overpressure after the peak overpressure is reached is not as drastic in the simulations as it was for the experiment. Since the drop-off in overpressure is more gradual in the simulation, the result is that there is more area under the curve and therefore the overpressure impulse is higher. The exception to this statement is the result of the 2D simulations at later times (especially Fig. 6, upper right, which is the 580-m sensor), where the predicted drop-off is very close to the experimental drop-off, which explains why the early part of the 2D predicted overpressure impulse curves for later times (e.g., Fig. 9, bottom) is very good. It is also noted that the 3D simulations predict the value of overpressure more accurately for early times (Fig. 10).

Another item of note pertaining to the overpressure impulse results shown in Fig. 9 is that the 2D simulation overpressure impulse values tend to agree better with the experiment for the initial part of the waveform (corresponding to the primary shock), while the 3D simulation overpressure impulse values tend to agree better with the experiment for the later part of the waveform (corresponding to the secondary shock). We believe that the reason for the better performance of the 2D simulation for the part of the overpressure impulse waveform corresponding to the primary shock is the much smaller zone size for the 2D geometry. As mentioned previously, the initial 2D zone size was over 18 times smaller than the initial 3D zone size for the fine mesh simulations, and this trend of smaller zone size in 2D compared to 3D continued throughout the calculation, which allowed for much better shock capture and shock resolution. The 2D simulation predicted the drop-off from peak overpressure much better than the 3D simulation, which allowed for better overpressure impulse predictions in the vicinity of the primary shock. The reason for the better performance of the 3D simulation for the part of the overpressure impulse waveform corresponding to the secondary shock is that the 3D geometry was much closer to experiment, which allowed for the timing of the secondary shock to be captured more accurately, which translates to the portion of the overpressure impulse curve corresponding to the secondary shock being predicted better.

3.3 Secondary shock

As mentioned in the introduction, a unique characteristic of certain (geometry-dependent) conventional solid explosions is the formation of a secondary shock [9]. The secondary shocks were observed experimentally at all high-pressure, seismic and acoustic sensors during all Sayarim

Fig. 7 Shape of blast wave pressure contour from the 3D calculation at various times (distance from ground zero of blast wave front is also given): **a** 0.00971 s, 3.9 m; **b** 0.00110 s, 4.1 m; **c** 0.00239 s, 6.6 m; **d** 0.00592 s, 21 m; **e** 0.00953 s, 31 m; **f** 0.0134 s, **g** 0.05 s, 115 m; **h** 0.1 s, 140 m; **i** 0.75 s, 480 m

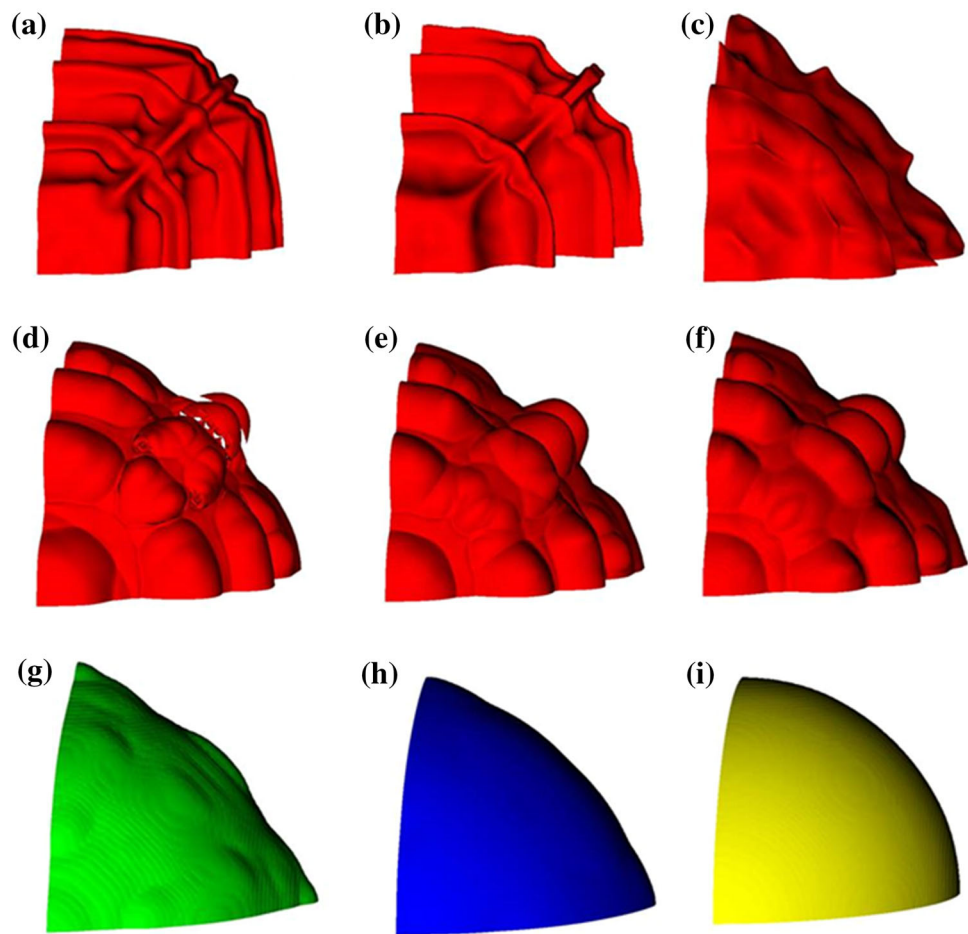
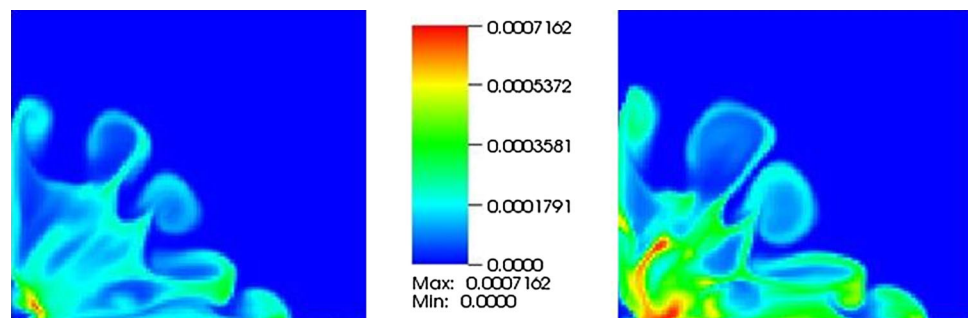


Fig. 8 Density contours (gm/cm^3 burnt explosive) of detonation products at 0.1 s (left) and 0.15 s (right). Results are from the 3D simulation taken at a slice through the center of detonation. Horizontal and vertical extents in the figure are approximately 150 m



surface explosions [12], and predicted in both the 2D and 3D (Figs. 5, 6) simulations.

Figure 11 shows flow visualization results from the 2D calculation for selected times during the numerical simulation. These plots help show the evolution of the secondary shock. The black dots in Fig. 11 are tracer particles that are initially located at the CompB/ANFO and ANFO/Air interfaces. At 8.753 ms (Fig. 11a), the primary detonation wave has turned into an air blast wave that is located at a distance of approximately 28 m from ground zero (recall the initial charge radius was 4 m). The tracer particles initially located at the CompB/ANFO interface have been displaced to a dis-

tance of 4 m from ground zero, and the tracer particles initially located at the ANFO/Air interface have displaced with the primary shock to a distance of approximately 24 m from ground zero. Kelvin–Helmholtz instabilities, which occur at interfaces in fluids when shear velocities exist at the interface [9], are seen to perturb the tracer particles at the ANFO/Air interface to a non-uniform pattern. At this time of 8.753 ms, a reflected shock is also seen at the origin (denoted by the high-pressure area at the origin, distinct from the high-pressure primary shock front).

At a time of 95.758 ms (Fig. 11b), the primary shock wave is located at a distance of approximately 105 m from ground

Fig. 9 Overpressure impulse vs. time for sensors 103 and 203 m from ground zero (*upper left*), 303 and 405 m from ground zero (*upper right*), 513 and 580 m from ground zero (*bottom*), 2D and 3D fine mesh simulations

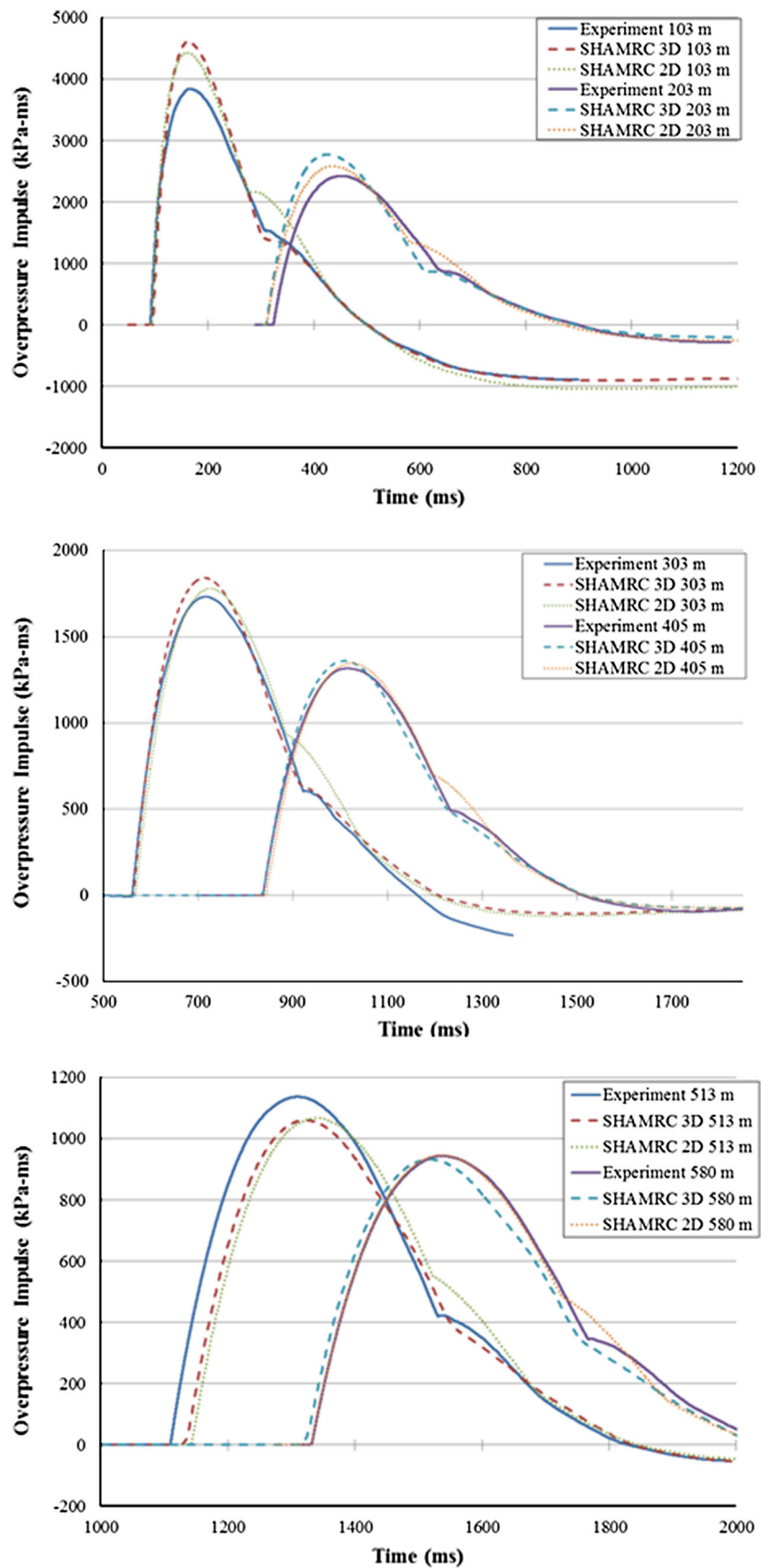


Table 4 Numerical comparison of select parameters between experiment and simulation for overpressure impulse, 2D and 3D

Sensor (m)	Experiment impulse _{max} (kPa-ms)	3D simulation impulse _{max} (kPa-ms)	3D simulation percent difference in impulse _{max} (%)	2D simulation impulse _{max} (kPa-ms)	2D simulation percent difference in impulse _{max} (%)
103	3840	4613	20.1	4420	15.1
203	2427	2772	14.2	2586	6.6
303	1731	1841	6.4	1779	2.8
405	1317	1358	3.1	1344	2.1
513	1138	1062	-6.7	1069	-6.1
580	945	931	-1.5	945	0.0

Only fine mesh simulation results are considered

zero (which corresponds to the primary shock arrival time at the 103-m sensor seen in Fig. 5, upper left). A secondary area of high pressure is again seen near the origin, with the wave front roughly at a distance of 15 m from ground zero. The high-pressure area near the origin at 95.758 ms is highly non-uniform, a result of the complex interactions between the detonation products and environment and interactions with the backward-facing shock. It is also seen at this time that the tracer particles initially located at both the CompB/ANFO and ANFO/Air interfaces are highly chaotic, as their paths have also been influenced by the complex interactions of the detonation products.

At a time of 200 ms (Fig. 11c), the primary shock wave is very clearly formed and is located at a distance of approximately 160 m from ground zero. The secondary shock wave is also clearly formed at this time, and is seen to be located at a distance of approximately 70 m from ground zero (note that experimentally, the secondary shock does not arrive at the 103-m sensor until a time of approximately 300 ms from detonation). Also seen at this time of 200 ms is that the primary shock has broken away from the tracer particles and therefore no longer has any influence over their paths.

4 Conclusions

This report has described numerical simulations of a 100-ton ANFO detonation, which were conducted using the government-owned code SHAMRC and compared to experiment. Both 2D and 3D simulations were conducted and yielded overpressure and impulse waveforms that agreed qualitatively with experiment, including the capture of the observed secondary shock.

The 2D simulation initial conditions assumed that the explosive masses were concentric hemispheres with the CompB inside the ANFO; the explosive mass was consistent between the experiment and simulation. The 2D simulation predicted the primary shock arrival time correctly, although the predicted secondary shock arrival time was early. The 2D

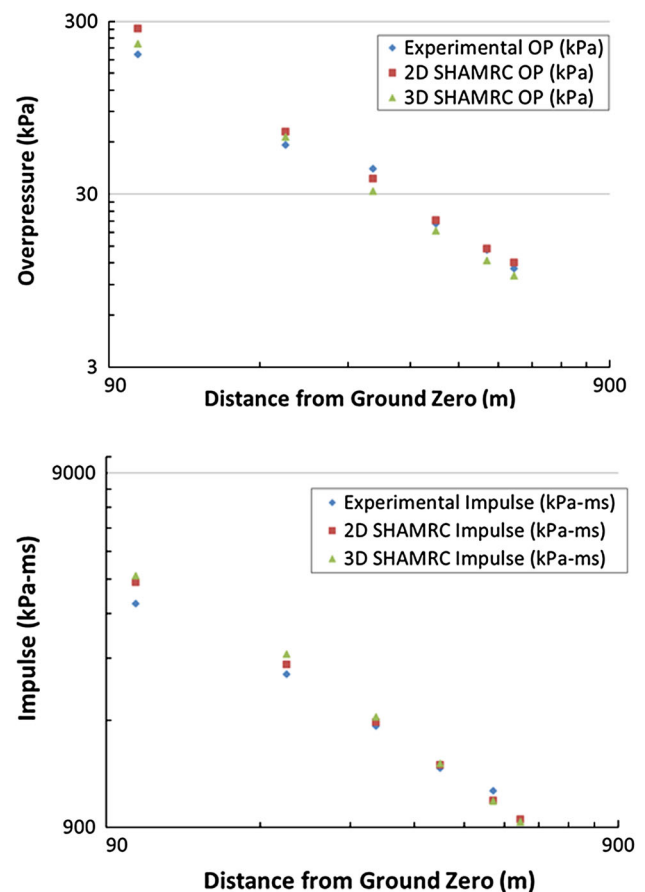


Fig. 10 Overpressure (*top*) and overpressure impulse (*bottom*) versus distance from ground zero, 2D and 3D fine mesh simulations. Please note that a logarithmic scale has been used

simulation overpressure impulse waveforms agreed very well with the experiment, especially at later calculation times, and prediction of the early part of the impulse waveform (associated with the initial peak) was better quantitatively for 2D compared to 3D. Therefore, the 2D simulation was found to capture the major experimental phenomena observed with a very good degree of accuracy.

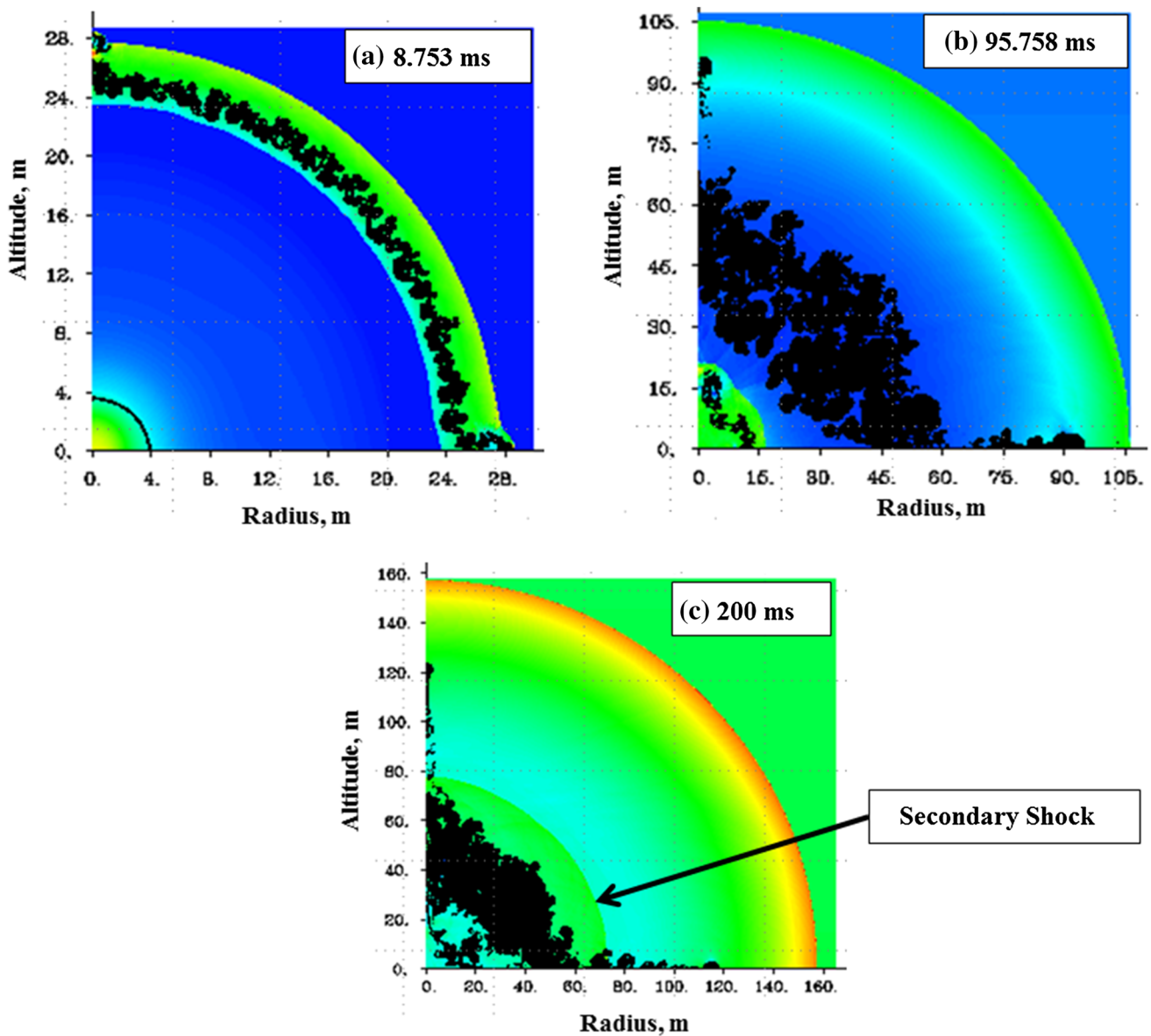


Fig. 11 Pressure contours at various times from 2D axisymmetric simulation. *Black dots* are tracer particles that are initially located at the Comp B/ANFO and ANFO/Air interfaces. The agglomeration of particles along the radius and altitude axes seen at later times are numerical artifacts

The 3D simulation initial conditions assumed that the experimental geometry could be represented as quarter-hemispherical with symmetric boundary conditions (a slight deviation from experiment) to reduce the run time. The 3D representation captured the relevant features of the experimental geometry (including the CompB being interspersed in the main ANFO mass). The 3D simulation also predicted the primary shock arrival time correctly, and secondary shock arrival times in 3D were closer to the experiment than the 2D results, likely due to the more accurate representation of the charge. The 3D-predicted overpressure impulse waveform had better quantitative agreement than 2D for the later part of the impulse waveform (associated with the secondary shock).

Zone-size sensitivity studies were conducted for both the 2D and 3D simulations. It was found that increasing the zone count from 16 million to 225 million in 2D and from 512 million to 1.728 billion in 3D did not affect the results significantly.

The final determination as to whether a 2D or 3D simulation is preferred is a matter of engineering judgment. Since the 2D simulation overpressure impulse results were found to agree more closely with experiment for the initial portion of the impulse wave (up until the secondary shock arrival), it may be argued that information lost in formulating the 2D assumption is not critical if the initial part of the overpressure impulse wave is the primary concern. If detailed capture of the experimental overpressure waveforms (to include accu-

rately predicting arrival time of the secondary shock) is of concern, then the 3D simulation is preferred.

Additionally, if there are features in the simulation that are inherently 3D, such as numerous buildings of varying sizes located in the path of the blast wave at varying distances, a 3D simulation would be required, so understanding differences in code behavior between 2D and 3D is important. The results of this numerical study show that SHAMRC may be reliably used to predict phenomena associated with the Sayarim 100-ton explosive detonation. The results provide very good accuracy and indicate that the code is well suited for predicting the outcomes of future explosive detonations.

Acknowledgments The authors would like to thank Dr. Phillip Cole and Dr. Paul Blake of the Defense Threat Reduction Agency (DTRA) for their leadership. Additionally, the authors would like to thank Dr. Jessie Bonner of Weston Geophysical Corporation for assistance with the experimental data. This work was sponsored under DTRA contract number DTRA01-03-D-0014-0038.

References

- Luccioni, B.M., Ambrosini, R.D., Danesi, R.F.: Analysing explosive damage in an urban environment. *Proc. I. Civil Eng. Struct. Build.* **158**, 1–12 (2005)
- Pierazzo, E., Melosh, H.J.: Hydrocode modeling of Chicxulub as an oblique impact event. *Earth Planet. Sci. Lett.* **165**, 163–176 (1999)
- Benselama, A.M., William-Louis, M.J.-P., Monnoyer, F., Proust, C.: A numerical study of the evolution of the blast wave shape in tunnels. *J. Hazard. Mater.* **181**, 609–616 (2010)
- Zhou, X.Q., Hao, H.: Prediction of airblast loads on structures behind a protective barrier. *Int. J. Impact Eng.* **35**, 363–375 (2008)
- Luccioni, B.M., Ambrosini, R.D., Danesi, R.F.: Analysis of building collapse under blast loads. *Eng. Struct.* **26**, 63–71 (2004)
- Crepeau, J., Happ, H.J., Hikida, S., Needham, C.E.: Second-order Hydrodynamic Automatic Mesh Refinement Code. Volume 2: User's Manual. Version 6. Applied Research Associates, Inc., Albuquerque (2011)
- Crepeau, J., Needham, C., Caipen, T., Grady, D., Harper, F.: First principles calculations of the interaction of blast waves with aqueous foams. In: Furnish, M.D., Chhabildas, L.C., Hixson, R.S. (eds.) *CP505, Shock Compression of Condensed Matter*, pp. 779–782. American Institute of Physics, USA (1999)
- Zukas, J.: *Introduction to Hydrocodes*. Elsevier Ltd., Oxford (2004)
- Needham, C.E.: *Blast Waves*. Springer, Berlin (2010)
- US Department of the Army: *Technical Manual (TM) 5-855-1: Fundamentals of Protective Design for Conventional Weapons*. Washington, DC (1986)
- Sochet, I., Gardebas, D., Caldeara, S., Marchal, Y., Longuet, B.: Blast wave parameters for spherical explosives detonation in free air. *Open J. Sci. Saf. Technol.* **1**, 31–42 (2011)
- Gitterman, Y., Hofstetter, R.: GT0 explosion sources for IMS infrasound calibration: charge design and yield estimation from near-source observations. *Pure Appl. Geophys.* **171**, 599–619 (2014). doi:[10.1007/s00024-012-0575-4](https://doi.org/10.1007/s00024-012-0575-4)
- US Government Printing Office: *US Standard Atmosphere, 1962*. Washington, DC (1962)
- Glasstone, S., Dolan, P.J.: *The Effects of Nuclear Weapons*, 3rd edn. United States Department of Defense and Energy Research and Development Administration, 653 p (1977)